Publishing Excellence
Inspiring Progress

ISSN: 3143-0732 https://aristonpubs.com/journal/science-of-alloys-and-glasses https://doi.org/10.69626/sag.2025.0072

RESEARCH ARTICLE

Erbium–Doped Oxyfluoride Tellurite Glass with Tailored Optical Properties for Compact Green Laser Sources

Raouia Lachheb [1], Kinga J.Kowalska [2], Bożena Burtan [3],Ibrahim Hadadi [4], Fawaz Alqahtani [4], Zahrah S.A Almutawah [5], Badriah Sultan [5,*]

ABSTRACT: This study reports on the synthesis and detailed optical characterization of a novel oxyfluoride tellurite glass system with the base composition $62TeO_2$-$5K_2TeO_3$-$20ZnO$-$10Nb_2O_5$-$3PbF_2$, activated with varying concentrations of Er_2O_3 at 2.0, 3.0, and 4.5 mol percent. The glasses were fabricated using the conventional melt-quenching technique. A comprehensive analysis of their luminescence behavior was undertaken, with key spectroscopic parameters including radiative transition probabilities, branching ratios, radiative lifetimes, and both absorption and emission cross-sections being systematically evaluated. Among the prepared samples, the glass containing 4.5 mol% Er_2O_3 demonstrated particularly promising characteristics. For the important $4I13/2 \rightarrow 4I15/2$ transition centered at 1.53 micrometers, this sample exhibited a notably high emission cross-section of $5.447 \times 10{-}21$ square centimeters and an optical gain coefficient of 5.03 per centimeter. Furthermore, this glass composition achieved exceptional quantum efficiency values, reaching 95 percent for the visible $4S3/2 \rightarrow 4I15/2$ transition and 93 percent for the near-infrared $4I13/2 \rightarrow 4I15/2$ transition. The Judd-Ofelt intensity parameters ($\Omega\lambda$, where λ takes values of 2, 4, and 6) were derived from the absorption spectra, providing insight into the local environment surrounding the erbium ions and the overall spectroscopic quality of the host matrix. The calculated spectroscopic quality factor, represented by the ratio $\Omega4/\Omega6$, fell within the range of 1.03 to 1.05. The fabricated glasses displayed intense visible green emission alongside broad near-infrared luminescence. Analysis of the emission colors using the Commission Internationale de l'Éclaierge chromaticity diagram revealed coordinates and correlated color temperatures that were highly consistent across all doped samples, firmly establishing their potential as efficient gain media for compact green-emitting solid-state laser applications.

Keywords: Oxyfluoride Tellurite Glass; Erbium Doping; Judd-Ofelt Analysis; Green Laser; Near-Infrared Luminescence; Quantum Efficiency.

Received: 12 December 2024; Revised: 27 January 2025; Accepted: 12 March 2025; Published Online: 24 March 2025

[1] Laboratory of Systems Integration and Emerging Energies, National Engineering School of Sfax (ENIS), University of Sfax, Sfax 3018, Tunisia.
[2] Faculty of Materials Science and Ceramics, AGH – University of Krakow, al. A. Mickiewicza 30, 30-059, Cracow, Poland.
[3] Institute of Physics, Cracow University of Technology, ul. Podchorazych 1, 30-084 Cracow, Poland.
[4] Department of Radiological Sciences, College of Applied Medical Sciences, King Khalid University, AlQuraa, Abha, P. O. Box 906, Saudi Arabia.
[5] Department of Physics, College of Sciences, King Khalid University, AlQuraa, Abha, P. O. Box 906, Saudi Arabia.

* Author to whom correspondence should be addressed: bsoltan@kku.edu.sa (Badriah Sultan)

1. INTRODUCTION

The relentless pursuit of advanced materials for photonic technologies has positioned glass science at the forefront of modern materials research. Among the vast family of glass-forming systems, tellurite-based glasses have emerged as

© Ariston Publications 2025. All rights reserved.

particularly compelling candidates for a wide array of optical applications, ranging from nonlinear optical devices to fiber amplifiers and solid-state laser sources [1, 2]. What makes tellurite glasses especially attractive is their unique combination of physical and optical properties. Tellurium dioxide (TeO_2) serves as a conditional glass network former, exhibiting a low phonon energy of approximately 760 cm^{-1}, which is considerably lower than that of conventional silicate, borate, or phosphate glasses. This characteristic is of paramount importance for rare-earth ion doping, as lower phonon energies minimize non-radiative multiphonon relaxation rates and thereby enhance the quantum efficiency of radiative transitions [3]. Additionally, tellurite glasses possess high refractive indices, excellent transparency from the visible to the mid-infrared region, and good chemical durability along with remarkable thermal stability [4, 5].

The incorporation of heavy metal oxides and fluorides into tellurite glass networks has been extensively explored as a strategy to further tailor their properties. The addition of Nb_2O_5, for instance, has been shown to significantly enhance both the linear and nonlinear optical characteristics of the host glass while simultaneously improving its thermal stability against crystallization [6]. Similarly, ZnO plays a crucial role as a glass modifier, contributing to network stabilization and influencing the local coordination environment around dopant ions [7]. However, despite these favorable attributes, conventional tellurite glasses face certain limitations. One persistent challenge is the presence of hydroxyl (OH) groups, which act as efficient quenching centers for rare-earth luminescence, particularly in the mid-infrared spectral region [8]. The high vibrational frequency of OH groups provides an effective pathway for non-radiative energy transfer from excited rare-earth ions, thereby reducing emission intensities and shortening fluorescence lifetimes. Furthermore, the fabrication of low-loss tellurite glass fibers has proven difficult due to issues related to material inhomogeneity and devitrification tendencies during fiber drawing [9].

In response to these challenges, researchers have turned their attention to oxyfluoride tellurite glass systems. These hybrid materials combine the desirable attributes of oxide glasses, such as mechanical strength and chemical stability, with the low phonon characteristics of fluorides [10, 11]. The introduction of fluorine into the tellurite network through compounds like lead fluoride (PbF_2) serves multiple beneficial purposes. Due to its higher electronegativity compared to oxygen, fluorine expands the glass-forming range and disrupts the network connectivity, resulting in reduced viscosity and enhanced clarity. More importantly, fluoride ions can effectively react with hydroxyl groups during the melting process according to the reaction $OH^- + F^- \rightarrow O^{2-} + HF\uparrow$, thereby scavenging these deleterious impurities and significantly reducing the OH absorption bands in the infrared region [12, 13]. This OH scavenging effect is critical for achieving efficient infrared luminescence, as it removes one of the primary non-radiative decay channels. The incorporation of PbF_2 also contributes to lowering the overall phonon energy of the glass matrix, further suppressing non-radiative losses and promoting radiative emission from rare-earth dopants [14].

Among the trivalent rare-earth ions, erbium (Er^{3+}) occupies a position of exceptional importance in photonics. Its energy level structure, characterized by the 4I15/2 ground state and a series of well-defined excited states including 2H9/2, 2H11/2, 4S3/2, 4F9/2, 4I11/2, and 4I13/2, enables multiple radiative transitions spanning the visible and near-infrared regions [15, 16]. The 4I13/2→4I15/2 transition centered on 1.53 μm has garnered tremendous attention due to its coincidence with the minimum loss window of silica optical fibers, making erbium-doped fiber amplifiers indispensable components in modern wavelength-division multiplexing communication systems [17]. Beyond telecommunications, this particular transition finds applications in eye-safe lasers, remote sensing, and medical procedures where operation at this wavelength ensures minimal tissue damage while maintaining desirable transparency in biological tissues [18]. In the visible spectrum, the 4S3/2→4I15/2 transition around 546 nm yields green emission that is valuable for compact visible laser sources, display technologies, and biomedical imaging. The 2H11/2→4I15/2 transition near 525 nm and the 4F9/2→4I15/2 transition around 660 nm provide additional visible emission channels that can be exploited for multi-color applications and optical thermometry [19, 20].

The present study focuses on a carefully designed oxyfluoride tellurite glass system with the nominal composition $62TeO_2$-$5K_2TeO_3$-$20ZnO$-$10Nb_2O_5$-$3PbF_2$, activated with varying concentrations of Er_2O_3. Several considerations guided the selection of this particular composition. The use of K_2TeO_3 as a starting material introduces an interesting dynamic during the melting process, as it undergoes thermal decomposition according to the reaction $K_2TeO_3 \rightarrow TeO_2 + K_2O$, thereby contributing additional TeO_2 to the glass network while potassium oxide acts as a modifier that enhances glass formation and influences the local structure around rare-earth ions [21]. The substantial TeO_2 content ensures that the glass retains the desirable low phonon energy and high refractive index characteristics of tellurite systems. The inclusion of Nb_2O_5 and ZnO serves to enhance optical nonlinearity and luminescence properties while providing network stabilization. The addition of PbF_2 introduces the beneficial fluorine content that reduces OH impurities and lowers the phonon energy environment surrounding the Er^{3+} ions. The novelty of this work lies in the systematic investigation of how increasing Er_2O_3 concentration from 2.0 to 4.5 mol% influences the structural, physical, and optical properties within this specific oxyfluoride tellurite matrix. While erbium-doped tellurite glasses have been studied previously, the combination of this particular multi-component host composition with a detailed quantitative analysis of luminescence parameters including Judd-Ofelt intensity factors, radiative transition probabilities, branching ratios, radiative lifetimes, emission cross-sections, and optical gain coefficients provides comprehensive insight into the potential of these materials for practical laser applications.

© Ariston Publications 2025. All rights reserved.

Particular attention is devoted to evaluating the quantum efficiencies for both visible green emission and near-infrared emission, as these parameters directly determine the suitability of the material for device applications. The correlation between structural changes induced by increasing erbium concentration and the resulting optical performance offers valuable guidance for optimizing glass compositions for specific photonic applications. Through this investigation, we aim to establish whether this newly developed oxyfluoride tellurite glass can serve as an effective host material for compact green solid-state lasers and broadband near-infrared amplifiers.

2. EXPERIMENTAL DETAILS

2.1. Glass Synthesis

A series of oxyfluoride tellurite glasses with the nominal molar composition $62TeO_2$-$5K_2TeO_3$-$20ZnO$-$10Nb_2O_5$-$3PbF_2$ and doped with Er_2O_3 at concentrations of 2.0, 3.0, and 4.5 mol% was prepared using the conventional melt-quenching technique. High-purity raw materials including TeO_2 (99.99 %), K_2TeO_3 (99.9 %), ZnO (99.99 %), Nb_2O_5 (99.9 %), PbF_2 (99.9 %), and Er_2O_3 (99.99 %) were used as starting components without further purification. For each batch, accurately weighed quantities corresponding to approximately 15 g of the final glass were thoroughly mixed in an agate mortar to ensure homogeneous distribution of all constituents. The well-mixed batches were transferred to high-purity platinum crucibles with tight-fitting lids to minimize volatilization losses during melting. The crucibles were placed in an electric furnace and heated to 950°C at a rate of 10 °/min, maintaining this temperature for 30 min with occasional swirling to promote homogeneity of the melt. Special attention was given to the reaction involving K_2TeO_3, which undergoes thermal decomposition during melting according to $K_2TeO_3 \rightarrow TeO_2 + K_2O$, contributing additional TeO_2 to the glass network while potassium oxide acts as a modifier. The molten material was then rapidly poured onto a preheated stainless steel plate and immediately transferred to a graphite mold preheated to 340°C. The cast samples were annealed at this temperature for two hours to relieve internal stresses developed during the quenching process. Subsequently, the furnace was switched off, allowing the glasses to cool gradually to room temperature. All prepared glass samples appeared transparent, homogeneous, and free from visible bubbles or crystalline inclusions. The undoped sample, designated as Sample A, served as a reference, while the erbium-doped samples were labeled according to their Er_2O_3 content as Sample B (2.0 mol %), Sample C (3.0 mol %), and Sample D (4.5 mol %).

The detailed nominal compositions of the prepared glass samples along with their measured density and calculated molar volume values are presented in Table 1. A clear trend of increasing density from 5.5713 to 5.6214 g/cm^3 was observed as the Er_2O_3 content increased from 0 to 4.5 mol %. This progressive increase in density can be attributed to the replacement of lighter oxide components with the heavier erbium oxide, as well as the filling of interstitial voids within the glass network by erbium ions acting as network modifiers. The molar volume correspondingly increased from 29.05 to 30.48 cm^3/mol with higher erbium concentration, indicating an expansion of the glass network structure. This expansion suggests that the incorporation of Er^{3+} ions creates additional non-bridging oxygen species and modifies the connectivity of the tellurite network, leading to a more open structure despite the increase in overall density.

2.2. Density and Physical Property Measurements

Density measurements were performed at room temperature using a helium gas pycnometer (AccuPyc 1330,µm) operating with an accuracy of $\pm$0.0001 g/cm^3. This technique was selected because it eliminates errors associated with surface tension and wetting that can affect conventional liquid displacement methods. For each glass sample, multiple measurements were conducted, and the average value was recorded. The molar volume (Vm) for each glass composition was calculated from the measured density using the relationship $Vm = (\sum xi\ Mi) / \rho$, where xi represents the molar fraction of each component i, Mi denotes its molecular weight, and ρ is the experimentally determined density. These values are presented in Table 1 along with the detailed glass compositions.

Table 1. Nominal compositions (mol %), measured density (g/cm^3), and calculated molar volume (cm^3/mol) of the undoped and Er_2O_3-doped oxyfluoride tellurite glass samples.

Glass sample	TeO_2	K_2TeO_3	ZnO	Nb_2O_5	PbF_2	Er_2O_3	Density (g/cm^3) ±0.0001	V_m (cm^3.mol^{-1}) ±0.001
Sample A	62	5	20	10	3	0	5.5713	29.05
Sample B	62	5	20	10	3	2	5.5816	29.77
Sample C	62	5	20	10	3	3	5.5901	30.10
Sample D	62	5	20	10	3	4.5	5.6214	30.48

© Ariston Publications 2025. All rights reserved.

2.3. Optical Absorption Spectroscopy

For optical characterization, the obtained glass samples were carefully cut and polished to achieve flat, parallel surfaces suitable for spectroscopic measurements. The final thickness of the polished samples was maintained at approximately 0.67 cm. Optical absorption spectra were recorded at ambient temperature using a dual-beam spectrophotometer (JASCO V-570) equipped with both UV-Visible and near-infrared detectors. This instrument provides a spectral resolution of ±1 nm across the entire measurement range. Absorption measurements were conducted over the wavelength region extending from 190 to 2500 nm, covering all relevant absorption bands corresponding to transitions from the 4I15/2 ground state to various excited states of the Er^{3+} ions. The absorption coefficient α(ν) was subsequently calculated from the measured absorbance using the relation α(ν) = 2.303 × A(ν) / d, where A(ν) represents the absorbance at frequency ν and d is the sample thickness. Transmission spectra in the infrared region were also recorded to evaluate the hydroxyl group content, with particular attention given to the absorption band near 3000 nm associated with OH vibrational modes.

2.4. Luminescence and Lifetime Measurements

Photoluminescence spectra and fluorescence decay curves were acquired using a customized setup described in detail elsewhere [10]. The excitation source consisted of an optical parametric oscillator pumped by the third harmonic of a Q-switched Nd:YAG laser operating at 355 nm with a pulse width of approximately 10 ns and a repetition rate of 10 Hz. The OPO output was tunable across the visible and near-infrared regions, allowing selective excitation of specific Er^{3+} absorption bands. For the present study, excitation wavelengths of 380 nm and 980 nm were employed to populate the upper emitting levels. The emitted fluorescence was collected perpendicular to the excitation beam to minimize scattered light, dispersed by a monochromator with a spectral resolution of 0.5 nm, and detected using a thermoelectrically cooled photomultiplier tube for visible emission or an InGaAs detector for near-infrared measurements. The signal was processed by a digital storage oscilloscope connected to a computer for data acquisition and analysis. Fluorescence decay curves were recorded by averaging multiple pulses to improve the signal-to-noise ratio, and the lifetimes were determined by fitting the decay profiles to single exponential functions. All luminescence measurements were performed at room temperature under identical experimental conditions to ensure reliable comparison between samples.

3. RESULTS AND DISCUSSION

3.1. Physical parameters

Incorporating Er_2O_3 into the glass matrix $62TeO_2$-$5K_2TeO_3$-$20ZnO$-$10Nb_2O_5$-$3PbF_2$ causes an increase in density value from 5.5713 to 5.6214 g/cm^3. This is due to increased coordination numbers and reduced interstitial gaps in the crosslinked glass matrix. The following parameters describe the physical properties of glass samples as: oxygen packing density (*OPD*), molar volume (V_m), and oxygen molar volume (V_o). These values are calculated using the following equation [6, 7].

$$V_m = \left(\frac{\sum i x_i m_i}{\rho_{glass}}\right) \quad (1)$$

$$V_o = V_m.\left(\frac{1}{x_i n_i}\right) \quad (2)$$

$$OPD = \sum i \frac{100.\rho_{glass}.n_i}{M_i} \quad (3)$$

Concerning each oxide, n_i denotes the number of oxygen atoms, m_i is the molecular weight of the glassy composition, and x_i is the molar fraction of the element. The molar refraction (R_m) and molar polarizability (α_m), which are dependent on the linear refractive index, n, and Vm, are calculated using the following equations:

$$R_m = V_m \frac{(n+1)(n-1)}{n^2+2} \quad (4)$$

$$\alpha_m = \left(\frac{3}{4(3.14)N_A V_m}\right).\left(\frac{n^2+2}{n^2-1}\right) \quad (5)$$

$$M = \frac{3}{n^2+2} \quad (6)$$

Where *M*, is the metallization criterion, Avogadro number (NA), and by using the linear optical susceptibility, the third-order nonlinear optical susceptibility, denoted as; $\chi^{(3)}$, may be found according to the below equationL

$$\chi^{(3)} = \left[\frac{(n^2-1)}{12.56}\right]^4 \times 10^{-10} \quad esu \quad (7)$$

The values of, V_m, V_o, and *OPD* of produced glasses are shown in Table 2. The molecular weight, bond length, oxygen atom concentration, coordination number, and cation radius of each glass component are the variables that contribute to these values, as reported in Table 2.

The unit structure of TeO_2 glasses consists of three phases which depend on the kind of modifier and intermediate oxide in the glass matrix [5]. The structural units are trigonal bipyramidal (TeO_4), polyhedron (TeO_{3+1}), and trigonal (TeO_3) designated Q_4^4, Q_4^3, and Q_3^2, respectively [5]. The number of bridging oxygens connected to the Te atom is superscripted, while the number of coordination oxygens surrounding is subscripted. Additionally, there may be an increase in TeO_{3+1} phases (Q_4^3) indicates that the glass networks increased elongation bridging. The, Er^+ ions fill the interstitial spaces, wich OPD decreased from 71.94 to 69.85 cm^3/mol. Table 3 reported the values R_m, α_m, M, and $\chi^{(3)}$ of

© Ariston Publications 2025. All rights reserved.

the fabricated glass. The values, R_m and α_m increased from 17.19 to 19.78 cm^3/mol and from 7.11 to 7.85 $Å^3$, respectively. The metallization criterion value, *M*, decreased from 0.383 to 0.379 as Er_2O_3 increased from 0 to 4.5 mol%. The value of, n, and $\chi^{(3)}$, increased from 2.214 to 2.2321, and 3.71 to 3.98 $\times 10^{-12}$ esu, respectively. The lowest value of α_m (7.85 $Å^3$) was reported for sample A, while sample D_4.5mol% Er_2O_3 recorded the highest value of α_m (5.623 $Å^3$). Incorporating Er_2O_3 into the host glass led to creating stretched bond Te-O_{ax}, breaking the chain formation from Te-O-Er and Te-O-Te bridges. Therefore, there are more lone pairs in the valence shell of Te^{4+} occupying the, sp3, hybrid orbital, due to the values of, α_m, and $\chi^{(3)}$, increased with the concentration of Er^{3+} ions increased.

3.2. Luminescence properties

The optical absorbance UV-VIS-NIR spectra of the produced glasses are estimated in Figure 1(a). It exhibits nine peaks at the wavelengths around 1508 nm, 976 nm, 796 nm, 648 nm, 544 nm, 522 nm, 488 nm, 450 nm, and 442 nm that correspond to the transition from the ground state of $^4I_{15/2}$ to the exited state of $^4I_{13/2}$, $^4I_{11/2}$, $^4I_{9/2}$, $^4F_{9/2}$, $^4S_{3/2}$, $^2H_{11/2}$, $^4F_{7/2}$,$^4F_{5/2}$ and $^4F_{3/2}$, respectively. The absorption spectra of the prepared doped glasses exhibit a similar band that increases with increasing erbium oxide concentration. The transition $^4I_{15/2} \rightarrow {}^4I_{13/2}$ is important for amplifiers operating in the 1500 nm communication window; moreover, the transition 4I15/2→2H11/2 is hypersensitive and strongly depends on covalence and site asymmetry [11], absorbing photon energy via the modifying ions (rare-earth and transition-metal) present in the oxide glasses. The formula $\alpha(v) = \frac{abs.}{d}$ was used to determine the optical absorption coefficient α(v). The inset in Figure 1(b) shows that the transmittance can exceed 90% and extends to 4.3 µm. At 3000 nm, there is a band that is thought to represent the normal absorption band for OH^-. It is well known that the OH group reduces emission intensity and durability by serving as a quenching site and thereby decreasing absorption [11, 12].

Table 2. The following physical parameters were measured for the prepared glass samples: oxygen molar volume (Vo) (cm3/mol), oxygen packing density (OPD) (g. atm/l), molar refraction (Rm) (cm^3/mol), αm,(Å3), metallization criterion (M), refractive index (n), third-order nonlinear optical susceptibility $\chi^{(3)}$, ×10-12 esu,, and concentration N, (1020 ions/cm^3).

Physical Parameters	Sample A	Sample B_2 2mol% Er	Sample C_ 3mol% Er	Sample D_ 4.5mol% Er
Concentration *N* (10^{20} ions/cm^3)	–	8.087	0.119	1.77
Oxygen molar volume, V_o, (cm^3/mol)	13.9	14.13	14.22	14.32
Oxygen packing density, OPD,g.atm/l	71.94	70.8	70.31	69.85
Molar refraction, R_m, (cm^3/mol)	17.92	18.76	19.17	19.78
Molar polarizability, α_m,($Å^3$)	7.11	7.45	7.61	7.85
Metallization criterion, M,	0.383	0.382	0.382	0.379
Refractive index, n,	2.214	2.218	2.2201	2.2321
Third-order nonlinear optical susceptibility, $\chi^{(3)}$, $\times 10^{-12}$ esu	3.71	3.78	3.8	3.98
Energy gap E_{opt}(eV)	2.937	2.9217	2.917	2.874

Table 3. JO intensity parameters of the prepared glasses compared to other types of glass.

Host glass	Ω_2 (pm^2)	Ω_4 (pm^2)	Ω_6 (pm^2)	Ω_4 / Ω_6	References
Sample B	1.021	0.631	0.600	1.05	This study
Sample C	1.116	0.642	0.621	1.03	This study
Sample D	2.401	0.951	0.914	1.04	This study
Phosphate	8.05	1.46	2.20	0.64	[23]
Tellurite	2.29	1.347	1.126	1.19	[24]
TG	1.20	1.14	1.35	0.84	[25]

© Ariston Publications 2025. All rights reserved.

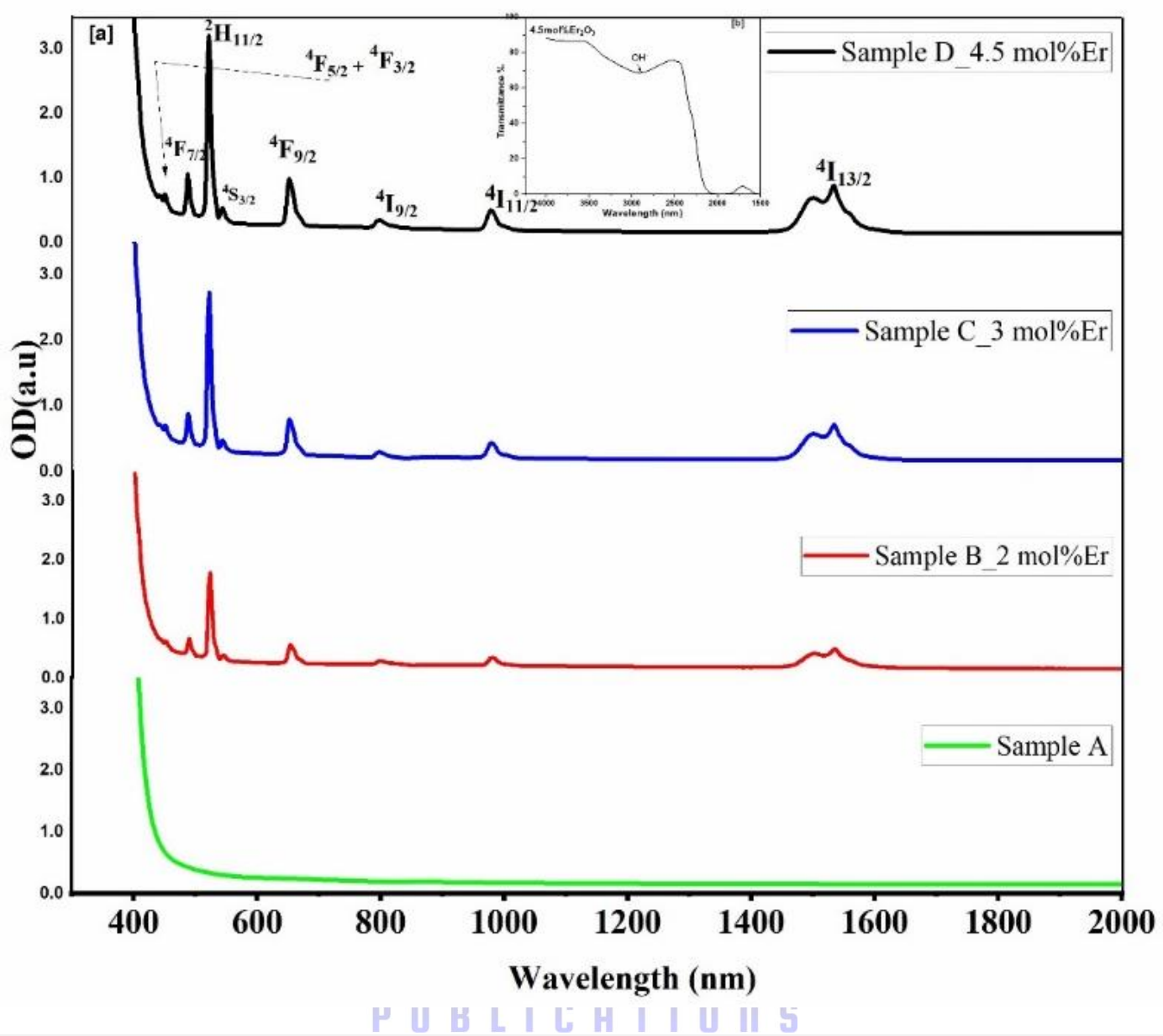

PUBLICATIONS

Fig.1. (a) UV-VIS-NIR spectra of the fabricated glass, and (b) Transmittance of produced glass sample D (4.5 mol% Er).

Fluoride ions can effectively replace hydroxide ions (OH-) during melting because they are isoelectronic and have similar ionic radii. The addition of fluorine may be explained by the fact that the OH^- absorption bands in the infrared transmittance spectra are less apparent. The equations $N_{OH} = \frac{A_v}{\epsilon_{OH}} \cdot \frac{1}{d} \ln(\frac{T_0}{T})$, $\alpha_{OH} = \frac{1}{d} \ln\left(\frac{T_0}{T}\right) at\ 3000\ nm$, in this context, A_v, for Avogadro's number, T_0/T denotes the relative transmittance of the glass sample, d, denotes the thickness of the glass sample, and, ϵ_{OH}, denotes the molar absorptivity of free OH groups. Since the value of ϵ_{OH}, for tellurite glasses has not been published yet, the value 49.1×10^3 cm^2/mol, which found in silicate glasses, is used [13]. In comparison to TY-4 glass (1.09 cm^{-1}) and TZN glass (0.75 cm^{-1}) [11], the produced glass's estimated α_{OH}, value of 0.71 cm^{-1} is low. Compared to BGGL [12], where $N_{OH}0=9.08\times10^{19}$ ions/cm was recorded, the produced glass had a residual hydroxyl ion (OH) concentration of 1.8×10^{17} ions/cm at 3000 cm. As a result, the produced glass is highly suitable for infrared fluorescence emission and offers the prospect of laser use.

Electron transitions occur in glass systems, where the glass sample thickness, d, is proportional to the energy difference between the valence and conduction bands (Eopt), which is determined by the energy gap in the glass. The following equation was used to determine it: $(\alpha hv) = A(hv - E_g)^r$. The variables. A, h, v, and r constants depend on the electronic transition process; r depends on the frequency, and h is Planck's constant. If we follow Tauc's relation, r = 1/2, it may occur for transitions that are permitted indirectly. Figure 2 shows a Tauc plot, from which Eopt is estimated by linear extrapolation. This figure displays $(\alpha hv)^{1/2}$ vs. (hv). Samples A and D_4.5mol% Er_2O_3 had a

© Ariston Publications 2025. All rights reserved.

decline in indirect optical band gap values, from 2.937 to 2.874 eV. The decrease in glass network rigidity is caused by the absorption band shifting to lower energy, resulting from the creation of elongation-bridging oxygen [7-8]. The glass matrix is stabilized by Er^{3+} ions, which have high coordination numbers and high polarizabilities. It follows that a reduction in the optical bandgap energy is caused by a decrease in the number of firmly bound valence electrons.

The JO theory is used to investigate optical amplification and the possibility of laser action in the prepared glasses [14-19]. The calculated electric and magnetic dipole line strengths (S_{ed}^{calc}, S_{md}) can be measured in form:

$$S_{ed}^{calc}(SLJ, S'L'J') = \sum_{k=2,4,6} \Omega_k \left|\langle SLJ \| U^{(k)} \| S'L'J' \rangle\right|^2 \quad (8)$$

And

$$S_{md}(SLJ, SLJ') = \left(\frac{h}{4\,\pi\, m\, c}\right)^2 |\langle SLJ \| L + 2S \| SLJ' \rangle|^2 \quad (9)$$

where $\langle \| U^{(k)} \| \rangle$ are the reduced matrix elements tabulated by Carnall et al [19] Ω_k (k=2, 4, 6) are the JO intensity parameters which can be calculated from the measured electric dipole line strengths (S_{ed}^{meas}) for the corresponding transitions between J and J' [17, 18]:

$$S_{ed}^{meas}(SLJ, S'L'J') = \frac{9n}{(n^2+2)^2}\left[4\pi\varepsilon_0 \frac{3ch\ (2J+1)}{8\pi^3 e^2} \times \frac{2.303}{LN\bar{\nu}} \int_{J\to J'} OD(\nu)\, d\nu - n\, S_{md}\right] \quad (10)$$

Quantum angular momentum totals for both initial and final states, denoted as J and J', respectively, L, represents the thickness of the prepared glasses, n, is the refractive index, $\int_{J\to J'} OD(\nu)d\nu$,is the integrated optical density within the corresponding wavelength range, ($\tilde{\nu}$ in cm^{-1}). Interactions between ions and their intermediate environments are associated with the JO intensity characteristics, which are governed by crystal-field parameters that affect the transition probability. Covalency between rare-earth ions and ligand anions has a substantial impact on the Ω_2 parameter, which is often sensitive to the symmetry of the rare-earth site. On the other hand, the stiffness of the host medium is connected to Ω_4 and Ω_6 [20, 21]. JO parameters of the samples are summarized in Table 3. The intensities of the JO parameters increase with Er_2O_3 oxide concentration. The factor $\Omega_4/\ \Omega_6$ for samples B, C, and D was found to be in the range of 1.05-1.03 and is listed in Table 3. Among the glasses listed in Table 3, the tellurite-based glass has the highest quality factor, whereas the prepared tellurite glasses have higher values than the phosphate and TG glasses.

The root mean square deviations δ_{rms} between the measured and the calculated electric dipole line strengths are listed in Table 4 and can be measured by:

$$\delta_{rms} = \left(\frac{\sum_{i=1}^{N_{trans}}\left(S_{ed}^{meas}(i) - S_{ed}^{cal}(i)\right)^2}{(N_{trans} - 3)}\right)^{\frac{1}{2}} \quad (10)$$

Where N_{trans} is the number of the transitions on the absorption spectra.

Once the JO parameters are measured, spectroscopic parameters can be evaluated, such as the radiative transition probabilities and the radiative lifetimes for J→J' transitions in spontaneous emission. All these parameters are registered in Table 5. Herein, the radiative lifetimes increase with the concentration of the erbium oxide. The radiative lifetimes, τrad, of the D-doped sample with 4.5 mol % Er_2O_3 were 2.35 ms for the transition 4S3/2•4I15/2 and 4.855 ms for the transition 4I13/2→4I15/2. Thus, the glass sample D can be a suitable host material for the laser emission at 1500 nm attributed to the interesting emission lifetime of $^4I_{13/2}\rightarrow{}^4I_{15/2}$ transition level. With an excitation wavelength of 380 nm, Figure 3 displays the emission spectra of Er^{3+}-doped glass. It shows a strong emission band at 550 nm, 4S3/2 • 4I15/2, and two smaller emission bands at 525 nm and 650 nm, 2H11/2 → 4I15/2 and 4F5/2 → 4I13/2, respectively. Figure 4 displays a decay curve for the Er^{3+} emission band $^4S_{3/2}\rightarrow{}^4I_{15/2}$, which is stimulated at 380 nm and has a lifetime of τ_{exp} = 2.35 ms. The quantum efficiency (η) can be evaluated by using the relation; $\eta = {}^{\tau_{exp}}/_{\tau_{rad}}$ % [20-23].

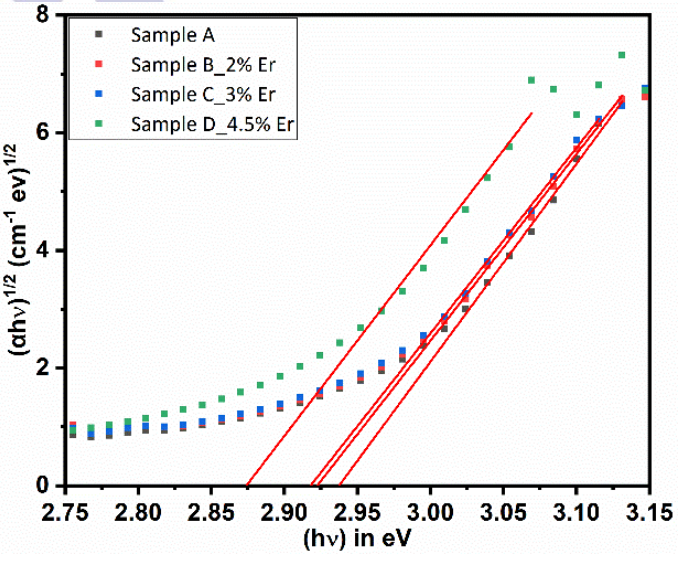

Fig. 2. $(\alpha h\nu)^{1/2}$ vs. $(h\nu)$ for the produced glasses.

Therefore, the quantum efficiency of visible emission for $^4S_{3/2}\rightarrow{}^4I_{15/2}$, ($\eta = 95\%$), The incorporation of 4.5 mol% Er^{3+} ions into the host glass network $62TeO_2$-$5K_2TeO_3$-$20ZnO$-$10Nb_2O_5$-$3PbF_2$ increases the quantum efficiency. The energy transfer between Er- Er ions, which delays emission, is responsible for the initial increase in lifetime with concentration.

© Ariston Publications 2025. All rights reserved.

Table 4. Measured and calculated ($S_{ed}^{meas}, S_{ed}^{calc}$) electric dipole line strengths for the prepared glasses.

Transition from $^4I_{15/2}$ to	Sample B_2mol%Er		Sample C_3mol%Er		Sample D_4.5mol%Er	
	S_{ed}^{meas} (pm^2) ±0.07	S_{ed}^{calc} (pm^2) ±0.04	S_{ed}^{meas} (pm^2) ±0.15	S_{ed}^{calc} (pm^2) ±0.04	S_{ed}^{meas} (pm^2) ±0.10	S_{ed}^{calc} (pm^2)
$^4I_{13/2}$	0.080	0.1515	0.177	0.252	0.1122	0.1863
$^4I_{11/2}$	0.150	0.449	0.178	0.74	0.1632	0.521
$^4I_{9/2}$	0.0989	0.1097	0.702	1.12	0.0563	0.1088
$^4F_{9/2}$	0.3414	0.3564	0.406	3.94	0.3815	0.3464
$^4S_{3/2}$	0.0414	0.089	0.088	0.24	0.0426	0.147
$^2H_{11/2}$	0.9891	0.9918	1.068	1.57	0.9073	0.9096
$^4F_{7/2}$	0.1723	0.279	2.310	6.23	0.2002	0.2334
$^4F_{5/2}$	0.0348	0.090	4.230	7.506	0.0433	0.0349
$^4F_{3/2}$	0.0112	0.051	1.220	2.96	0.0148	0.0085
δ_{rms} (pm^2)	0.21×10^{-6}		0.26×10^{-6}		0.28×10^{-6}	

Table 5. The radiative lifetimes (τrad), branching ratios (β, and spontaneous emission probabilities (Aed) of the glass samples were measured at each energy level.

Transitions	Sample B_2mol% Er			Sample C_3mol% Er			Sample D_4.5mol% Er		
	A_{ed} (s^{-1})	β(%)	τ_{rad} (ms)	A_{ed} (s^{-1})	β(%)	τ_{rad} (ms)	A_{ed} (s^{-1})	β(%)	τ_{rad} (ms)
$^4I_{13/2}\rightarrow{}^4I_{15/2}$	206	`100	4.268	216	100	4.634	234	100	4.855
$^4I_{11/2}\rightarrow{}^4I_{15/2}$	36	13.52	2.685	37	10.25	3.319	38	12.28	3.691
$\rightarrow{}^4I_{13/2}$	234	86.47		264	89.74		334	87.71	
$^4I_{9/2}\rightarrow{}^4I_{15/2}$	6	3.99	4.055	5	3.201	4.159	6	3.698	4.396
$\rightarrow{}^4I_{13/2}$	10	6.129		15	11.54		23	8.676	
$\rightarrow{}^4I_{11/2}$	147	89.87		154	85.26		175	87.62	
$^4F_{9/2}\rightarrow{}^4I_{15/2}$	14	1.459	0.883	14	1.341	1.104	15	1.577	1.040
$\rightarrow{}^4I_{13/2}$	47	4.907		45	4.286		50	5.200	
$\rightarrow{}^4I_{11/2}$	123	12.81		147	18.71		212	16.29	
$\rightarrow{}^4I_{9/2}$	776	80.81		696	75.65		856	76.92	
$^4S_{3/2}\rightarrow{}^4I_{15/2}$	1	0.185	1.710	1	0.346	2.131	2	0.265	2.471
$\rightarrow{}^4I_{13/2}$	9	2.273		15	4.239		25	3.252	
$\rightarrow{}^4I_{11/2}$	10	2.567		14	3.382		19	2.973	
$\rightarrow{}^4I_{9/2}$	351	86.87		387	78.34		458	82.63	
$\rightarrow{}^4F_{9/2}$	32	8.10		51	13.68		80	10.87	
$^2H_{11/2}\rightarrow{}^4I_{15/2}$	1	0.018	0.344	1	0.018	0.380	1	0.017	0.363
$\rightarrow{}^4I_{13/2}$	4	0.148		4	0.153		4	0.152	
$\rightarrow{}^4I_{11/2}$	48	1.759		51	1.752		51	1.794	
$\rightarrow{}^4I_{9/2}$	274	9.980		307	10.59		307	9.942	
$\rightarrow{}^4F_{9/2}$	1,150	41.76		1,233	42.50		1,233	39.97	
$\rightarrow{}^4S_{3/2}$	1,275	46.32		1,305	44.97		1,305	48.12	
$^4F_{7/2}\rightarrow{}^4I_{15/2}$	1	0.014	0.248	1	0.015	0.316	1	0.016	0.309
$\rightarrow{}^4I_{13/2}$	2	0.101		3	0.083		4	0.102	
$\rightarrow{}^4I_{11/2}$	76	2.363		67	1.968		79	2.423	
$\rightarrow{}^4I_{9/2}$	116	3.601		123	3.561		143	3.911	
$\rightarrow{}^4F_{9/2}$	65	2.031		63	1.749		70	1.999	
$\rightarrow{}^4S_{3/2}$	18	0.584		18	0.477		19	0.587	
$\rightarrow{}^2H_{11/2}$	2,946	91.30		2,876	92.14		3,706	90.95	

© Ariston Publications 2025. All rights reserved.

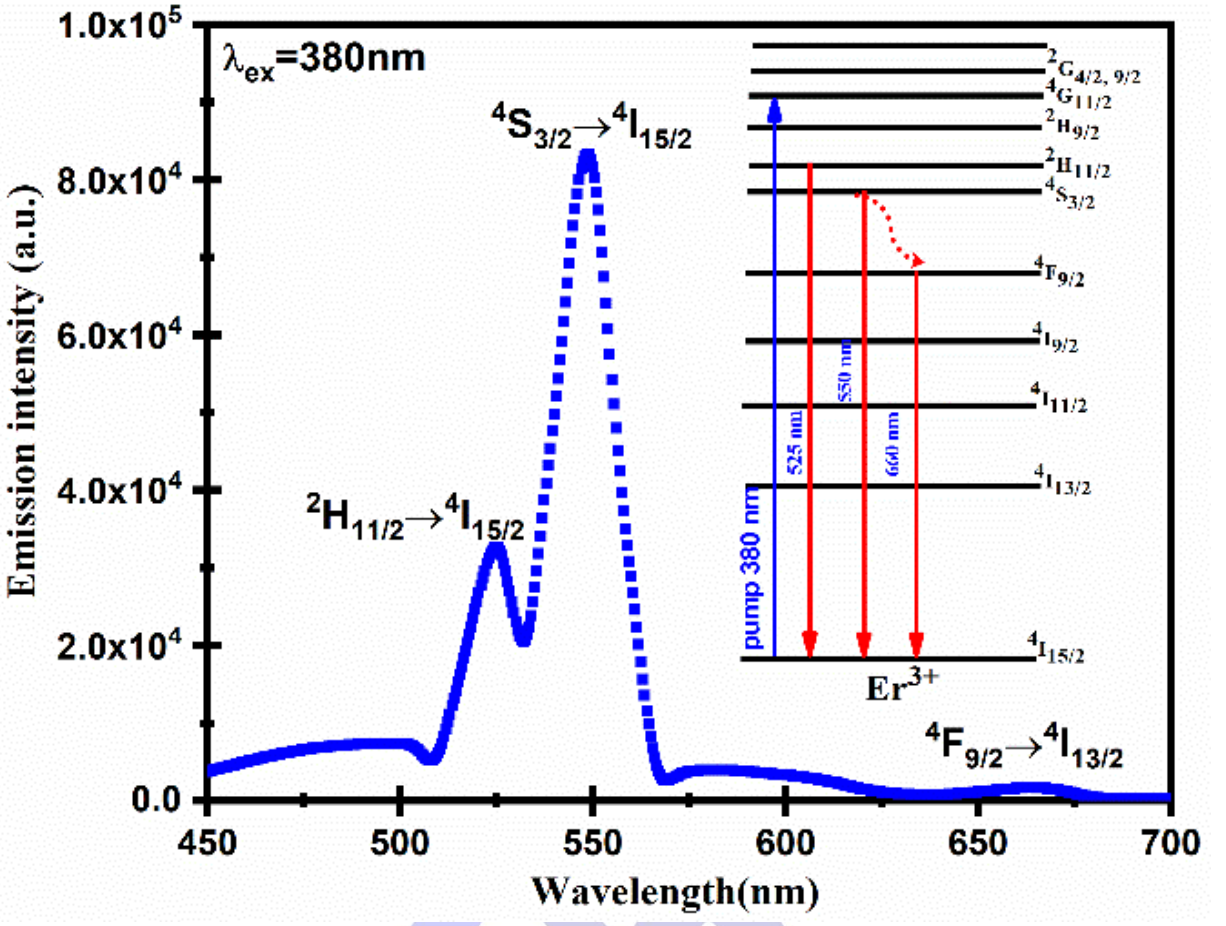

Fig. 3. The emission spectra of glass excited at 380 nm with 4.5 mol% Er^{3+}.

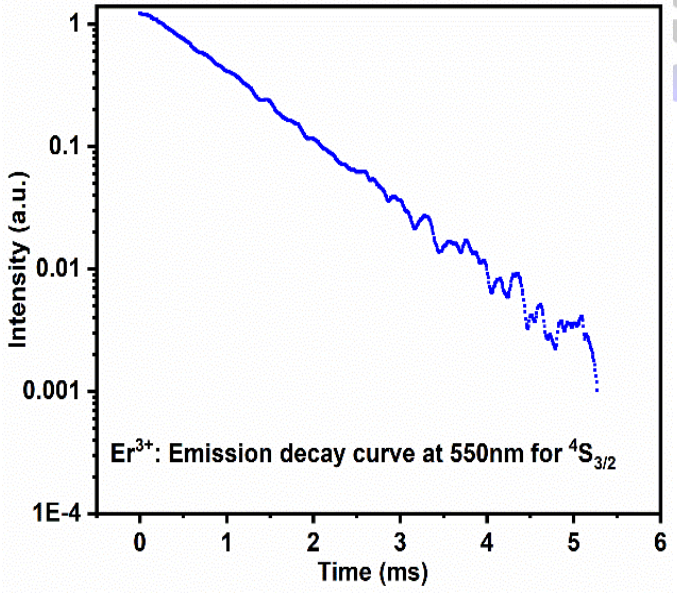

Fig. 4. Shows the 4.5mol% Er^{3+} doped glass emission transition decay graph at 550 nm, which corresponds to the $^4S_{3/2} \rightarrow {}^4I_{15/2}$ transition.

The greatest lifetime observed for sample D_4.5 Er mol% is consistent with the substantial spectrum expanding in extensively doped glasses, which also suggests that the rate of energy transfer increases with concentration of Er ions. It was shown that the lifetime increased more at low OH-concentrations than at high residual OH-concentrations. The results show that even at higher Er_2O_3 concentrations, the concentration-quenching effects are negligible. After de-excitation rates were initiated from the 4I13/2 level at high Er^{3+} ion concentration, it became clear that no ions were present in which relaxation could occur.

The emission spectra at excitation wavelength 980 nm obtain that the sample D_4.5mol% Er^{3+} has a wide near-infrared emission maximum at 1534 nm (Figure 5). Which corresponds to the transition from $^4I_{13/2}$ to $^4I_{15/2}$, with a full-width half maximum (FWHM) is 85 nm. Moreover, various bands that correspond to transitions from distinct $^4I_{13/2}$ Stark-split levels to the ground level were seen in Figure 5. At 1530 nm emission of the erbium-doped fiber amplifier (EDFA) used in the wavelength-division-multiplexing (WDM) optical communication network system, the width of the emission band at 1.54 μm is a crucial characteristic. The FWHM of 1.5 μm for Al/P silica is equal 44 nm [20],

© Ariston Publications 2025. All rights reserved.

fluorozirconate (65nm) [20, 21], borate bismuth glass (79 nm) [24], germinate glass (53 nm) [25], phosphate glass (37 nm) [26], tellurite glass (85 nm) [25- 28], silica glass (40 nm) [24], and ZBLAN glass (82 nm) [27] have been reported.

Figure 6 displays the luminescence decay curves of the produced glasses in the following $^4I_{13/2} \rightarrow {}^4I_{15/2}$ emission, and the value of fluorescence decay time is 4.512 ms. A decrease in nonradiative relaxation by ion-ion interaction in these glasses and surrounding ions in the initial state $(^4I_{15/2})$ re-absorb photons that relax spontaneously from the $^4I_{13/2}$ level.

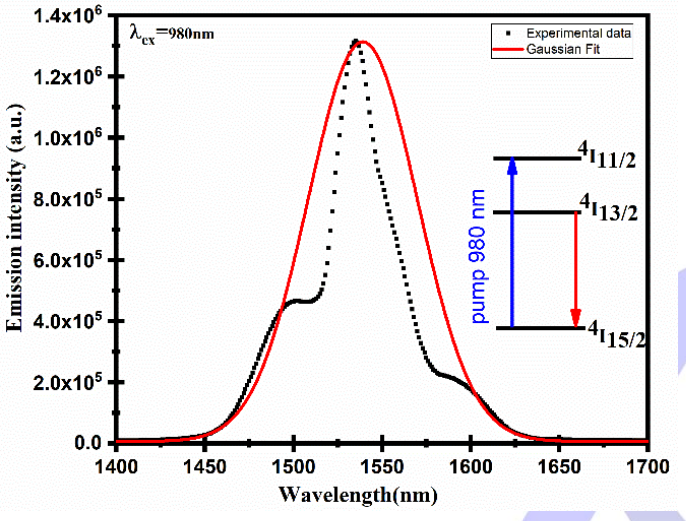

Fig. 5. The emission spectra of glass excited at 980 nm with 4.5 mol% Er^{3+}.

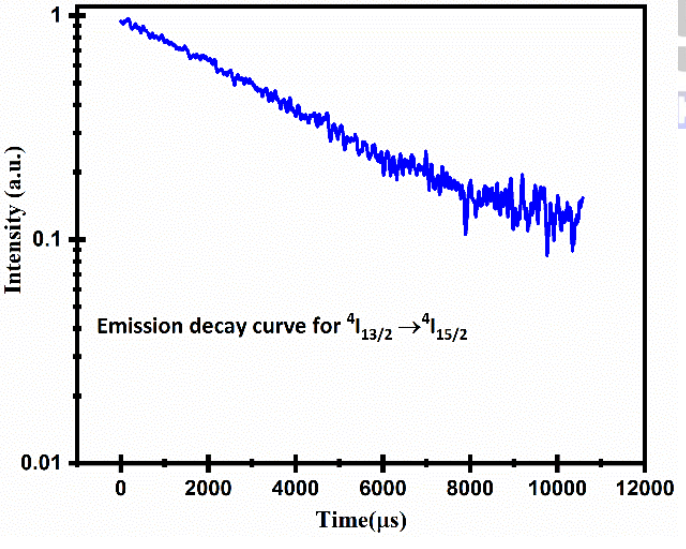

Fig. 6. Shows the 4.5mol%Er^{3+} doped glass emission transition decay graph, which corresponds to the $^4I_{13/2} \rightarrow {}^4I_{15/2}$ transition.

The value of quantum efficiency (η) of this transition level ($\eta = 93\%$), which indicated that the glass produced with added Er_2O_3 exhibits favorable optical properties. Incorporating Er^{3+} also increases the quantum efficiency and emission band intensity by producing additional non-bridging oxygens (NBO) in the TeO_{3+1} phase. This is a consequence of structural alterations, as shown on the Ω_2 parameter. Beyond that, the crystalline field around the Er^{3+} ions is changed by the structural changes of the matrices, leading to an increase in, η, when compared to glasses described in previous studies [21- 26]. Thus, these glasses show promise as hosts for laser fiber emission in the visible and near-infrared spectra, according to this study's findings. The electrons in the $^4I_{9/2}$ state were converted to the 4I11/2 state via multiphonon relaxation (MPR) because the energy difference between the two states is slight. The transition of Er^{3+} from $^4I_{11/2}$ to $^4I_{15/2}$ is partially relaxed to 4I15/2 via a 980 nm radiative emission.

Subsequently the $^4I_{13/2}$ state that is populated will emit a 1.53 µm photon via the transition of Er^{3+}, which is accompanied by a radiative emission of Er^{3+}: $^4I_{13/2} \rightarrow {}^4I_{15/2}$ + 1.53 µm. The absorption cross-section, σ_a, of sample D doped Er^{3+} ions for the $^4I_{13/2} \rightarrow {}^4I_{15/2}$ transition is estimated as follows:

$$\sigma_a(\lambda) = \frac{2.303\, log\left(\frac{I_0}{I}\right)}{NL} \qquad (11)$$

Where $\log(I_0/I)$ is the optical density. Thus, the emission cross-section can be evaluated using σ_a according to the McCumber theory [18, 19]:

$$\sigma_e(\lambda) = \sigma_a(\lambda)\ \frac{Z_l}{Z_u} exp\left[\frac{hc}{kT}\left(\frac{1}{\lambda_{ZL}} - \frac{1}{\lambda}\right)\right] \qquad (12)$$

Where Z_l/ Z_u is the ratio between the lower and the upper partition functions states and λ_{ZL} is the wavelength for the transition between the lower Stark sublevels of the emitting multiples and the lower Stark sublevels of the receiving multiplets.

The absorption and the emission cross-sections of the transition from level $^4I_{13/2}$ to level $^4I_{15/2}$ of the sample D doped with 4.5 mol% of Er_2O_3 are presented in Figure 7. They recorded a value respectively, $\sigma_a = 2.5\times10^{-20}$ cm^2 and $\sigma_e = 2.84\times10^{-20}$ cm^2 at the wavelength 1534 nm. The emission cross-section was found to be bigger than other tellurite glasses published by A. A. Assadi et al. [30]. Compared to phosphate glasses, which have a value of 7.6×10^{-21} cm^2, this value is 37% greater, in silicate glasses, it is 39% higher [30, 31].

The gain coefficient, $G((\lambda)$, is another interesting parameter for rare-earth doped glass. It can be measured as follows:

$$G(\lambda) = N\big(P.\sigma_e(\lambda) - (1-P).\sigma_a(\lambda)\big) \qquad (13)$$

Which, P, represents the population ratio of the higher state.

Figure 8 shows the gain coefficient as a function of the wavelength with different population inversions. With the total inversion case (P=1), the optical gain of the sample D

© Ariston Publications 2025. All rights reserved.

recorded a value equal to 5.03 cm^{-1} at 1534 nm. Thus, this tellurite glass is a promising gain material for near-infrared broadband amplifiers.

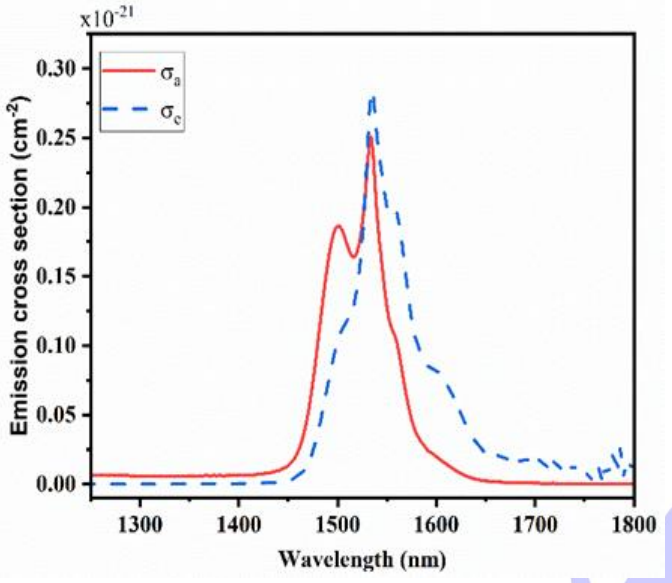

Fig 7. Absorption, σ_a, and stimulated emission cross-section σ_e of $^4I_{13/2} \rightarrow {}^4I_{15/2}$ transition of 4.5mol% Er_2O_3.

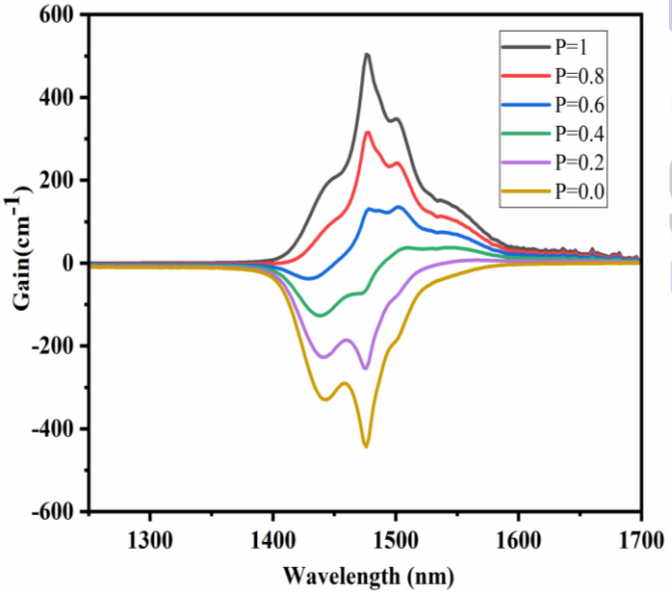

Fig. 8. Optical gain coefficient of the transition energy $^4I_{13/2} \rightarrow {}^4I_{15/2}$ of 4.5mol% Er_2O_3.

The CIE algorithm [33, 34] was used to obtain the green emission color of the prepared glass, with chromatic coordinates (x=0.269, y=0.603), (x=0.268, y=0.603), and (x=0.268, y=0.604) for sample B_2% Er, sample C_3% Er, and sample D_4.5% Er, respectively. The CIE coordinates obtained were approximately similar to those that occur naturally in cool green emission. The characteristic color created using McCamy's approximation method, which is shown in Figure 9, depends extensively on the computed color temperature (CCT) [35, 37],

$$CCT = \quad -449 \ (n^2 + 3525n - 6823.3)n + 5520.33 \quad (14)$$

Where, n=(x-0332)/(0.186-y), the CCT value refers to 6644, 6645, and 6646 K of sample B_2% Er, sample C_3% Er, and sample D_4.5% Er, respectively. Therefore, the produced glass has approximately the same values for both CIE coordinates and CCT, producing green light commonly found in commercial locations. The manufactured glasses are ideal for use as the green LED-emitting diodes ($_G$-LEDs) and as laser sources of intense task illumination.

4. CONCLUSION

A new series of oxyfluoride tellurite glasses with the composition $62TeO_2$-$5K_2TeO_3$-$20ZnO$-$10Nb_2O_5$-$3PbF_2$ and doped with Er_2O_3 at concentrations of 2.0, 3.0, and 4.5 mol% was successfully synthesized and thoroughly characterized. The systematic incorporation of erbium ions into the glass network induced significant changes in the material's physical properties. Increasing density, molar polarizability, refractive index, and third-order nonlinear optical susceptibility were observed with higher Er_2O_3 content, while both oxygen packing density and optical band gap energy decreased progressively. These structural modifications, driven largely by the creation of non-bridging oxygen species, directly contributed to the enhanced optical performance of the doped glasses. Application of the Judd-Ofelt theoretical framework to the absorption spectra yielded intensity parameters following the trend $\Omega2 > \Omega4 > \Omega6$ across all samples. The consistently high spectroscopic quality factor ($\Omega4/\Omega6$), ranging from 1.03 to 1.05 and peaking for the 4.5 mol% Er_2O_3-doped glass, indicates a favorable balance of radiative transition probabilities within the host material, confirming its suitability for hosting optically active rare-earth ions. The luminescence investigations proved most compelling. Under optical pumping, the glasses exhibited strong emission bands in both the visible green region centered at 550 nm (4S3/2→4I15/2 transition) and the near-infrared telecommunication window centered at 1.53 μm (4I13/2→4I15/2 transition). The glass doped with 4.5 mol% Er_2O_3 demonstrated exceptional performance, achieving remarkably high quantum efficiencies of 95% for the visible transition and 93% for the near-infrared transition. A fluorescence lifetime of 4.512 ms for the 4I13/2 level further confirmed the low phonon energy environment provided by the oxyfluoride matrix. The calculated emission cross-section reached 2.84 × 10−20 cm^2, with an optical gain coefficient of 5.03 cm^{-1} at 1534 nm under full population inversion.

© Ariston Publications 2025. All rights reserved.

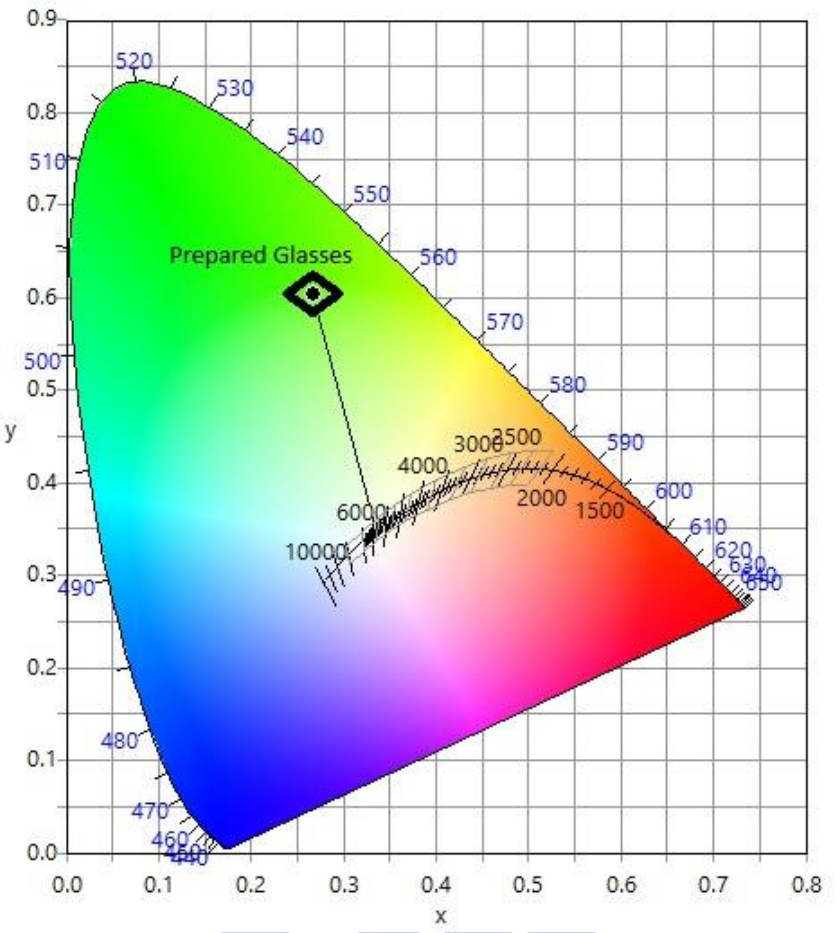

Fig. 9. Chromaticity diagram (CIE) and calculate color temperature (CCT) of prepared glasses.

The nearly identical Commission Internationale de l'Éclairage chromaticity coordinates (approximately x=0.268, y=0.603) and correlated color temperatures (around 6645 K) confirmed stable and pure green emission. This combination of high quantum efficiency, favorable gain characteristics, and color purity firmly establishes this erbium-doped oxyfluoride tellurite glass, particularly the composition with 4.5 mol% Er_2O_3, as a highly promising material for compact and efficient green solid-state lasers and advanced photonic devices.

DECLARATIONS

Ethical Approval

We affirm that this manuscript is an original work, has not been previously published, and is not currently under consideration for publication in any other journal or conference proceedings. All authors have reviewed and approved the manuscript, and the order of authorship has been mutually agreed upon.

Funding

Not applicable

Availability of data and material

The datasets used and/or analyzed during the current study are available from the corresponding author on reasonable request.

Conflicts of Interest

The authors declare that they have no financial or personal interests that could have influenced the research and findings presented in this paper. The authors alone are responsible for the content and writing of this article.

Authors' contributions

Raouia Lachheb: Conceptualization, Methodology, Formal analysis, Investigation, Writing—original; **Kinga J.Kowalska**: Conceptualization, Methodology, Investigation, Writing—original draft, Formal analysis, Writing—review and editing; **Bożena Burtan**: Methodology, Writing—

© Ariston Publications 2025. All rights reserved.

review and editing, Visualization; Writing—review and editing. **Ibrahim Hadadi**: Conceptualization, Methodology, Investigation, Writing—original draft, Formal analysis, Writing—review and editing; **Fawaz Alqahtani**: Formal analysis, Investigation, Writing—original draft, Writing—review and editing, Visualization; **Zahrah S.A Almutawah ;** Conceptualization, Methodology, Investigation, Visualization; **Badriah Sultan**: Methodology, Investigation, Visualization, review and editing.

ACKNOWLEDGMENTS

The authors extend their appreciation to University Higher Education Fund for funding this research work under Research Support Program for Central labs at King Khalid University through the project number CL/PRI/B/3.

REFERENCES

[1] Yang, D.L., Gong, H., Pun, E.Y.B., Zhao, X. and Lin, H., **2010**. Rare-earth ions doped heavy metal germanium tellurite glasses for fiber lighting in minimally invasive surgery. *Optics Express*, 18(18), pp.18997-19008.

[2] Lin, J., Huang, W., Sun, Z., Ray, C.S. and Day, D.E., **2004**. Structure and non-linear optical performance of TeO_2–Nb_2O_5–ZnO glasses. *Journal of Non-Crystalline solids*, 336(3), pp.189-194.

[3] Yousef, E., Hotzel, M. and Rüssel, C., **2004**. Linear and non-linear refractive indices of tellurite glasses in the system TeO_2–WO_3–ZnF_2. *Journal of Non-Crystalline Solids*, 342(1-3), pp.82-88.

[4] Chen, F., Wei, T., Jing, X., Tian, Y., Zhang, J. and Xu, S., **2015**. Investigation of mid-infrared emission characteristics and energy transfer dynamics in Er^{3+} doped oxyfluoride tellurite glass. *Scientific Reports*, 5(1), p.10676.

[5] Hoppe, U., Yousef, E., Rüssel, C., Neuefeind, J. and Hannon, A.C., **2004**. Structure of zinc and niobium tellurite glasses by neutron and x-ray diffraction. *Journal of Physics: Condensed Matter*, 16(9), pp.1645-1663.

[6] Boussetta, A., Al-Syadi, A.M., Albargi, H.B., Damak, K., Ersundu, A.E., Ersundu, M.Ç., Ramadan, E., Alshehri, A.M., Hussein, K.I., Maalej, R. and Yousef, E.S., **2024**. An investigation of the photonic application of TeO_2-K_2TeO_3-Nb_2O_5-BaF_2 Glass Co-Doped with Er_2O_3/Ho_2O_3 and Er_2O_3/Yb_2O_3 at 1.54 μm based on its thermal and luminescence properties. *Materials*, 17(17), p.4188.

[7] Chen, F., Wei, T., Jing, X., Tian, Y., Zhang, J. and Xu, S., **2015**. Investigation of mid-infrared emission characteristics and energy transfer dynamics in Er^{3+} doped oxyfluoride tellurite glass. *Scientific Reports*, 5(1), p.10676.

[8] Yousef, E.S.S., **2005**. Characterization of oxyfluoride tellurite glasses through thermal, optical and ultrasonic measurements. *Journal of Physics D: Applied Physics*, 38(21), pp.3970-3975.

[9] Chen, G.X., Zhang, Q.Y., Yang, G.F. and Jiang, Z.H., 2007. Mid-infrared emission characteristic and energy transfer of Ho^{3+}-doped tellurite glass sensitized by Tm^{3+}. *Journal of Fluorescence*, *17*(3), pp.301-307.

[10] Burtan-Gwizdala, B., Reben, M., Cisowski, J., Lisiecki, R., Jarząbek, B., Alshehri, A., Hussein, K.I. and Yousef, E.S., **2023**. Enhanced emission of tellurite glass doped with Pr^{3+}/Ho^{3+} and their applications. Materials, 16(3), p.925.

[11] Rivera, V.A.G., El-Amraoui, M., Ledemi, Y., Messaddeq, Y. and Marega Jr, E., **2014**. Expanding broadband emission in the near-IR via energy transfer between Er^{3+}–Tm^{3+} co-doped tellurite-glasses. *Journal of Luminescence*, 145, pp.787-792.

[12] Schab-Balcerzak, E., Siwy, M., Kawalec, M., Sobolewska, A., Chamera, A. and Miniewicz, A., **2009**. Synthesis, characterization, and study of photoinduced optical anisotropy in polyimides containing side azobenzene units. *The Journal of Physical Chemistry A*, 113(30), pp.8765-8780.

[13] Lachheb, R., Damak, K., Assadi, A.A., Herrmann, A., Yousef, E., Rüssel, C. and Maâlej, R., **2015**. Characterization of Tm3+ doped TNZL glass laser material. *Journal of Luminescence*, 161, pp.281-287.

[14] Tsuda, M., Soga, K., Inoue, H., Inoue, S. and Makishima, A., **1999**. Upconversion mechanism in Er 3+-doped fluorozirconate glasses under 800 nm excitation. *Journal of Applied Physics*, 85(1), pp.29-37.

[15] Charfi, B., Damak, K., Maâlej, R., Alqahtani, M.S., Hussein, K.I., Alshehri, A.M., Hussain, A.M., Burtan-Gwizdala, B., Reben, M. and Yousef, E.S., **2022**. Enhancement of optical telecommunication bands: Pr^{3+}-doped halide phosphate glasses display broadband NIR photoluminescence emission. *Materials*, 15(19), p.6518.

[16] Seneschal, K., Smektala, F., Bureau, B., Le Floch, M., Jiang, S., Luo, T., Lucas, J. and Peyghambarian, N., **2005**. Properties and structure of high erbium doped

 © Ariston Publications 2025. All rights reserved.

phosphate glass for short optical fibers amplifiers. *Materials Research Bulletin*, 40(9), pp.1433-1442.

[17] BR, J., **1962**. Optical absorption intensities of rare-earthions. *Physical Reviews*, 127, pp.750-761.

[18] Ofelt, G.S., **1962**. Intensities of crystal spectra of rare-earth ions. *The Journal of Chemical Physics*, 37(3), pp.511-520.

[19] Carnall, W.T., Fields, P.R. and Rajnak, K., **1968**. Electronic energy levels of the trivalent lanthanide aquo ions. III. Tb3+. *The Journal of Chemical Physics*, 49(10), pp.4447-4449.

[20] Linganna, K., Suresh, K., Ju, S., Han, W.T., Jayasankar, C.K. and Venkatramu, V., **2015**. Optical properties of Er3+-doped K-Ca-Al fluorophosphate glasses for optical amplification at 1.53 μm. *Optical Materials Express*, 5(8), pp.1689-1703.

[21] Babu, S., Seshadri, M., Prasad, V.R. and Ratnakaram, Y.C., **2015**. Spectroscopic and laser properties of Er3+ doped fluoro-phosphate glasses as promising candidates for broadband optical fiber lasers and amplifiers. *Materials Research Bulletin*, 70, pp.935-944.

[22] Jiang, X., Lousteau, J., Shen, S. and Jha, A., **2009**. Fluorogermanate glass with reduced content of OH-groups for infrared fiber optics. *Journal of Non-Crystalline Solids*, 355(37-42), pp.2015-2019.

[23] Liao, M., Hu, L., Duan, Z., Zhang, L. and Wen, L., **2007**. Spectroscopic properties of fluorophosphate glass with high Er^{3+} concentration. *Applied Physics* B, 86(1), pp.83-89.

[24] Tian, Y., Xu, R., Hu, L. and Zhang, J., **2011**. Effect of chloride ion introduction on structural and 1.5 μm emission properties in Er^{3+}-doped fluorophosphate glass: publisher's note. *Journal of the Optical Society of America B*, 28(11), pp.2701-2701.

[25] Feng, X., Tanabe, S. and Hanada, T., **2001**. Hydroxyl groups in erbium-doped germanotellurite glasses. *Journal of Non-Crystalline Solids*, 281(1-3), pp.48-54.

[26] Dai, S., Wu, J., Zhang, J., Wang, G. and Jiang, Z., **2005**. The spectroscopic properties of Er^{3+}-doped TeO_2–Nb_2O_5 glasses with high mechanical strength performance. *Spectrochimica Acta Part A: Molecular and Biomolecular Spectroscopy*, 62(1-3), pp.431-437.

[27] Manikandan, N., Ryasnyanskiy, A. and Toulouse, J., **2012**. Thermal and optical properties of TeO_2–ZnO–BaO glasses. *Journal of Non-Crystalline Solids*, 358(5), pp.947-951.

[28] Damodaraiah, S., Prasad, V.R. and Ratnakaram, Y.C., **2018**. Investigation of Green and 1.53 μm emission characteristics of Er^{3+} doped bismuth phosphate glasses for laser applications. *Journal of Alloys and Compounds*, 741, pp.269-280.

[29] Alhakami, M.H., Abouhaswa, A.S., Althubiti, N.A. and Taha, T.A.M., **2025.** Investigation of optical and radiation shielding properties in bismuth oxide-doped barium borate glasses. *Nuclear Engineering and Technology*, *57*(9), p.103633.

[30] Assadi, A.A., Damak, K., Lachheb, R., Herrmann, A., Yousef, E., Rüssel, C. and Maâlej, R., **2015**. Spectroscopic and luminescence characteristics of erbium doped TNZL glass for lasing materials. *Journal of Alloys and Compounds*, 620, pp.129-136.

[31] Lin, H., Pun, E.Y.B. and Liu, X.R., **2001**. Er^{3+}-doped Na2O· $Cd_3Al_2Si_3O_{12}$ glass for infrared and upconversion applications. *Journal of Non-Crystalline Solids*, 283(1-3), pp.27-33.

[32] Ohtsuki, T., Peyghambarian, N., Honkanen, S. and Najafi, S.I., **1995**. Gain characteristics of a high concentration Er^{3+}-doped phosphate glass waveguide. *Journal of Applied Physics*, 78(6), pp.3617-3621.

[33] Kashif, I. and Ratep, A., **2025**. Various color light emission from single, double, and triple Eu 3+/Tb 3+/Tm 3+ doped borate glass excited by UV light. *Journal of Fluorescence*, 35(1), pp.343-355.

[34] Hasabeldaim, E.H.H., Swart, H.C. and Kroon, R.E., **2023**. Luminescence and stability of Tb doped CaF_2 nanoparticles. *RSC Advances*, 13(8), pp.5353-5366.

[35] Maheshwari, K. and Rao, A.S., **2022**. Photoluminescence downshifting studies of thermally stable Dy3+ ions doped phosphate glasses for photonic device applications. *Optical Materials*, 129, p.112518.

[36] Xu, S., Fu, J., Liu, X., Yuan, M., Zhang, C., Wang, H., Liu, G. and Cui, S., **2023**. Analysis of thermal chromaticity stability, energy transfer and colour tunablity of Dy^{3+}-Eu^{3+} doped BBZL glasses for high-power W-LED applications. *Ceramics International*, 49(3), pp.5228-5238.

[37] Rajaramakrishna, R., Nijapai, P., Kidkhunthod, P., Kim, H.J., Kaewkhao, J. and Ruangtaweep, Y., **2020**. Molecular dynamics simulation and luminescence properties of Eu^{3+} doped molybdenum gadolinium borate glasses for red emission. *Journal of Alloys and Compounds*, 813, p.151914.

© Ariston Publications 2025. All rights reserved.